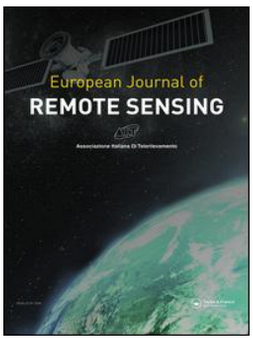

European Journal of Remote Sensing

ISSN: (Print) 2279-7254 (Online) Journal homepage: https://www.tandfonline.com/loi/tejr20

Quantifying the impact of trees on land surface temperature: a downscaling algorithm at city-scale

Elena Barbierato, Iacopo Bernetti, Irene Capecchi & Claudio Saragosa

To cite this article: Elena Barbierato, Iacopo Bernetti, Irene Capecchi & Claudio Saragosa (2019): Quantifying the impact of trees on land surface temperature: a downscaling algorithm at city-scale, European Journal of Remote Sensing, DOI: 10.1080/22797254.2019.1646104

To link to this article: https://doi.org/10.1080/22797254.2019.1646104

Published online: 29 Jul 2019.

EUROPEAN JOURNAL OF REMOTE SENSING
https://doi.org/10.1080/22797254.2019.1646104

Taylor & Francis
Taylor & Francis Group

FROM SPACE TO LAND MANAGEMENT

OPEN ACCESS Check for updates

Quantifying the impact of trees on land surface temperature: a downscaling algorithm at city-scale

Elena Barbierato[a], Iacopo Bernetti[a], Irene Capecchi[a] and Claudio Saragosa[b]

[a]DAGRI, Department of Agriculture, University of Florence, Firenze, Italy; [b]DIDA, Department of Architecture, University of Florence, Firenze, Italy

ABSTRACT

The climate of a city influences the ways in which its outdoor spaces are used. Especially, public spaces intended for use by pedestrians and cyclists, such as parks, squares, residential and commercial streets, and foot and cycle paths will be used and enjoyed more frequently if they have a comfortable and healthy climate. Due to the predicted global temperature increase, urban climate is likely to become more uncomfortable, especially in summer when an increase in heat stress is expected. Urban forestry has been proposed as one approach for mitigating the human health consequences of increased temperature resulting from climate change. The aims of the current research were to (a) provide a transferable methodology useful for analyzing the effect of urban trees on surface temperature reduction, particularly in public spaces, and (b) provide high-resolution urban mapping for adaptation strategies to climate change based on green space projects. To achieve the established aims, we developed a methodology that uses multisource data: LiDAR data, high-resolution Landsat imagery, global climate model data from CMIP5 (IPPC Fifth Assessment), and data from meteorological stations. The proposed model can be a useful tool for validating the efficiency of design simulations of new green spaces for temperature mitigation.

ARTICLE HISTORY
Received 26 January 2019
Revised 22 June 2019
Accepted 16 July 2019

KEYWORDS
Land surface temperature (LST); climate change; light detection and ranging (LIDAR); urban forest; urban heat waves; climate change; land surface temperature; LiDAR; solar radiation; urban forest; urban heat island

Introduction

Cities are characterized by higher temperatures than surrounding rural areas and, as has been shown by numerous climatological studies, they also have higher temperatures than in the past (Rozbicki & Golaszewski, 2003). This phenomenon, called the urban heat island (UHI), is determined mostly by the materials from which the cities are built and by the greater anthropic activity carried out within them (Oke, 1973; Rizwan, Dennis, & Chunho, 2008; Roth, Oke, & Emery, 1989). The climate of a city influences the ways in which its outdoor spaces are used. Especially, public spaces intended for use by pedestrians and cyclists, such as parks, squares, residential and commercial streets, and foot and cycle paths are used and enjoyed more frequently when they have a comfortable and healthy climate. Due to the predicted global temperature rise, climate is likely to become more uncomfortable, especially in summer, when heat waves are very likely to increase in frequency and intensity, so an increase in heat stress is expected.

Urban forestry has been proposed as one solution to mitigate the human health consequences of increased temperature resulting from climate change. Several studies have focused specifically on the effects of trees, comparing temperatures in a site with trees with those of a nearby site without trees (Bowler, Buyung-Ali, Knight, & Pullin, 2010). The most used approach for investigating the role of urban trees on land surface temperature (LST) is based on multivariate spatial statistical models in which the normalized difference vegetation index (NDVI) is used as an explanatory variable (see Weng, Lu, & Schubring, 2004; Yuan & Bauer, 2007; Guo et al., 2015; Bonafoni, Anniballe, Gioli, & Toscano, 2016;; Zhao, Jensen, Weng, & Weaver, 2018). According to the literature, urban morphology also has an important role in shaping urban heat island phenomena; the relationship between LST and urban morphology has recently been analyzed using the Sky View Index (SVI) calculated based on 3D city models, which are derived from LiDAR data (Kokalj, Zakšek, & Oštir, 2011; Chun & Guldman, 2014; Tan, Lau, & Ng, 2016; Nakata-Osaki, Souza, & Rodrigues, 2018).

Mirzaei (2015, p. 204) in a review of UHI assessment methods at different scales, concludes that "despite the ability of mesoscale models to investigate the large-scale effect of the UHI, their accuracy is not efficient to provide details on the urban canopy layer and this gap therefore will require further research to develop spatially and computationally efficient models." Although the methods based on 3D modeling provide high-resolution estimates at a scale appropriate for urban planning, they do not allow the estimation of a reliable ground temperature value, especially during heat waves (Acero & Arrizabalaga, 2018; Lenzholzer &

CONTACT Iacopo Bernetti ibernetti@unifi.it DAGRI, Department of Agriculture, University of Florence, Firenze, Italy

Brown, 2016; Salvati, Monti, Roura, & Cecere, 2019). The SVI-based models must instead be combined with data from remote sensing to be able to take into account the effect of the evapotranspiration of urban green (Hodul, Knudby, & Ho, 2016; Scarano & Sobrino, 2015). Moreover, they are not easily usable for either the estimation of climatic anomalies or for projections on future scenarios of climate change.

For these reasons, the aims of this research were to (1) provide a replicable methodology useful for downscaling LST during heat waves to the scale used in city planning and projects to analyze the effect of urban trees on the reduction of surface temperature, particularly in public spaces; and (2) provide high-resolution urban mapping for adaptation strategies to climate change based on green space projects to reduce heat-related risks to the vulnerable population.

Materials and methods

Study area

This research was applied in the city of Rosignano Solvay a small city of Central Italy located on the Tuscan coast and overlooking the Tyrrhenian Sea. The study area has boundary coordinates (datum WGS84, projection UTM, zone 32) N min = 613253, N max = 618615, E min = 4803895, E max = 4807895, and mean latitude = 43.39° N.

Since the aim of the research is based on quantifying the effect of urban forest in the city, the perimeter of the study area excludes areas in which this effect is not suitable and sufficient to mitigate the urban microclimate. Thus, industrial areas to the south of the city, some neighboring areas that are too far from the city center and those that are on the border with rural areas have been excluded from the municipal territory (Figure 1).

The study area covers an area of 586 100 hectares, which 224 257 ha of urban green and the remaining part by artificial surface.

The territory of Rosignano Solvay falls in the "Hot-summer Mediterranean climate" class according to the classification of Köppen and Geiger. Regions with this form of the Mediterranean climate typically experience hot, sometimes very hot and dry summers. In this season the population, 20 340 total inhabitants, is very vulnerable to heat waves, in particular, the categories most at risk for heat-related health are the following: 27.57% are people over 65, 9.85% are widowed, 46.14% have low education, and finally 5.68% are rented families.

Datasets

Thermal synthesis information can be acquired using remote sensing techniques through sensors operating in the thermal infrared band (TIR) installed on both airborne and satellite platforms. Such remote sensing thermal images are widely used for the study of urban landscapes because they provide a synoptic and synchronous grid of temperature data, allowing the analysis of urban problems related to local climate and the UHI (Rajeshwari & Mani, 2014). In this study, we used data from the thermal infrared sensor of Landsat 8 (bands 10 and 11) with a spatial resolution of 30 m. The image used for the evaluation of the UHIs in the current climatic conditions was based on the analysis of the temporal variability of the anomaly of the maximum daily temperature, calculated through the time series from 2004 to 2018 of the daily maximum temperatures referred to the meteorological station of Quercianella. To identify dates with heat waves, we used the 95th percentile of the frequency distribution of the daily maximum temperature (Anderson &

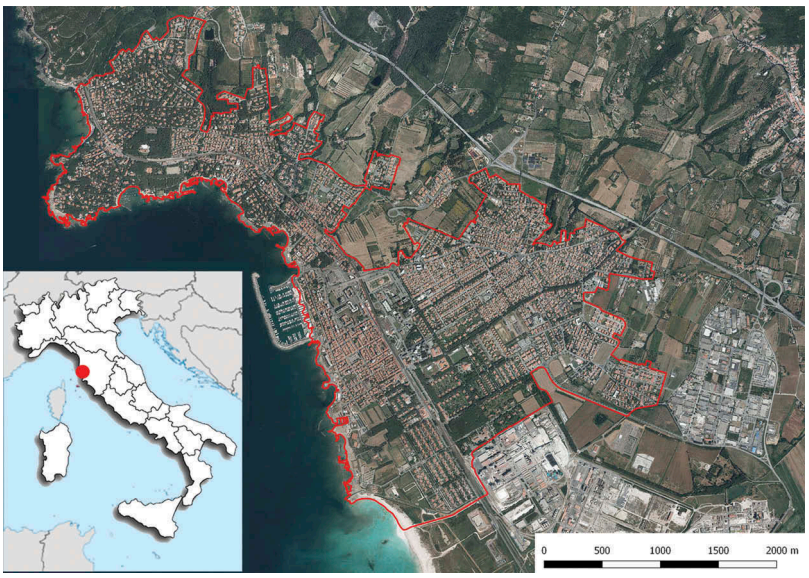

Figure 1. The region of interest.

Bell, 2009; D'Ippoliti et al., 2010) in the 14 years considered. Based on the quality of the Landsat 8 images, the day of 8 August 2017, was chosen. To obtain the LST related to the chosen image, the QGIS Land Surface Temperature Estimation Plugin was used (Isaya Ndossi & Avdan, 2016).

The climate change data were derived from the WorldClim open access downscaling models (Hijmans, Cameron, Parra, Jones, & Jarvis, 2005) based on the Coupled Model Intercomparison Project Phase 5 models. The model chosen was the GFDL-ESM2G model (Dunne et al., 2012), with reference year of 2050. The dataset had a spatial resolution of 30 seconds of longitude and latitude (about 670 × 930 m at the latitude of the study area).

The urban vegetation coverage was derived from the NDVI processed using 15 aerial multispectral frames (four bands: red, green, blue, and near infrared) acquired in December 2012 by means of an UltraCam Xp (Vexcel) digital metric camera with a resolution of 0.2 × 0.2 m. The digital elevation model (DEM) of the urban canopy layer was derived from 20 LiDAR images with a resolution 1 × 1 m acquired in 2008. The LiDAR data were provided by the Italian Ministry of the Environment, Land and Sea. The points acquired from this survey have an altimetric accuracy of ± 15 cm and a planimetric accuracy is ± 30 cm. In this work, the data available by the geographical portal of the Tuscan region with a resolution of 1 × 1 meter were used. That resolution was considered satisfactory for the objectives of the work. Following Konijnendijk (2003), we defined urban forest as all forest and tree resources in urban areas, which comprises all of the trees in public and private spaces, along linear routes and waterways, and in amenity areas. Thus, the urban forest map was calculated through a map overlay of NDVI and LiDAR DEM data, with trees defined as the NDVI cells with height greater than 4 m.

Methodology

There are two main approaches for downscaling climate data: dynamical and statistical (Benestad, Hanssen-Bauer, & Chen, 2008; Trzaska & Schnarr, 2014). Dynamical downscaling applies climate models based on physical principles to reproduce local climate over a finer grid by solving equations of motion and thermodynamics. On the other hand, statistical downscaling establishes empirical relationships between local climate-dependent variables and a set of known independent variables or predictors.

In this work, we applied to the urban area a method for downscaling temperature maps using the solar radiation falling in the urban canopy layer estimated from LiDAR data of the study area. Figure 2 shows the graphical workflow of the research.

Many authors have demonstrated through physical models the relationship between radiant flux and surface temperature in urbanized territories (see Myrup, 1969; Nunez & Oke, 1977; Oke, 1988; Mirzaei, 2015). In particular, George, Thompson, and Faaborg (2015) verified the relationship between LST and small-scale solar radiation using a low-cost temperature logger network and airborne LiDAR to develop a dynamic high-resolution spatio-temporal temperature model to be used in site-level ecological studies. Our method is a modified version of the approach proposed originally by Felicísimo Pérez and Martín-Tardío (2018) for use in species distribution modeling, and it is based on the hypothesis that solar energy is a main factor driving local temperature variability especially in days of heat wave when the sky is generally without clouds.

Solar radiation estimation

The core of the method consists of estimating an urban morphology index derived from the incident solar radiation that can be applied to the DEM of the urban canopy layer with cell size of 1 m to downscale the Landsat LST with cell size of 30 m.

The first step is to estimate the direct and diffuse solar irradiation over each 1 m DEM cell. These variables were estimated using the r.sun module of the GRASS and QGIS systems (Mitasova & Neteler, 2008).

The inputs of the r.sun procedure are DEM, Julian day corresponding to the Landsat image (220th day) and local time (10 a.m. corresponding to acquisition time). The result is output in kJ/m^2 as a gridded map of potential solar radiation values with a spatial resolution that is the same as that of the DEM used. The total solar radiation is the sum of the direct and diffuse components at ground level. To take into account the effect of trees on solar radiation under the canopy, we used the following map overlay procedure:

$$R^G = \begin{cases} R^D + R^B & \text{cells not covered by canopy of trees} \\ R^D & \text{cells covered by canopy of trees} \end{cases}$$

where R^G is ground solar radiation, R^D is diffuse solar radiation, and R^B is direct solar radiation.

The following step involves the estimation of the urban morphology index (symbolized as μ) from the previously estimated solar radiation. The rationale for this estimation is that the μ values will indicate how much the LST of each cell should be modified based on its exposure to solar radiation. The estimation of topographic indexes from solar radiation was performed by applying the directly proportional relationship between energy E radiated per unit surface area of a black body across all wavelengths per unit time and the fourth power of the black body's thermodynamic temperature T:

$$E = \sigma \cdot T^4$$

where σ is the Stefan–Boltzmann constant. The index μ was calculated as

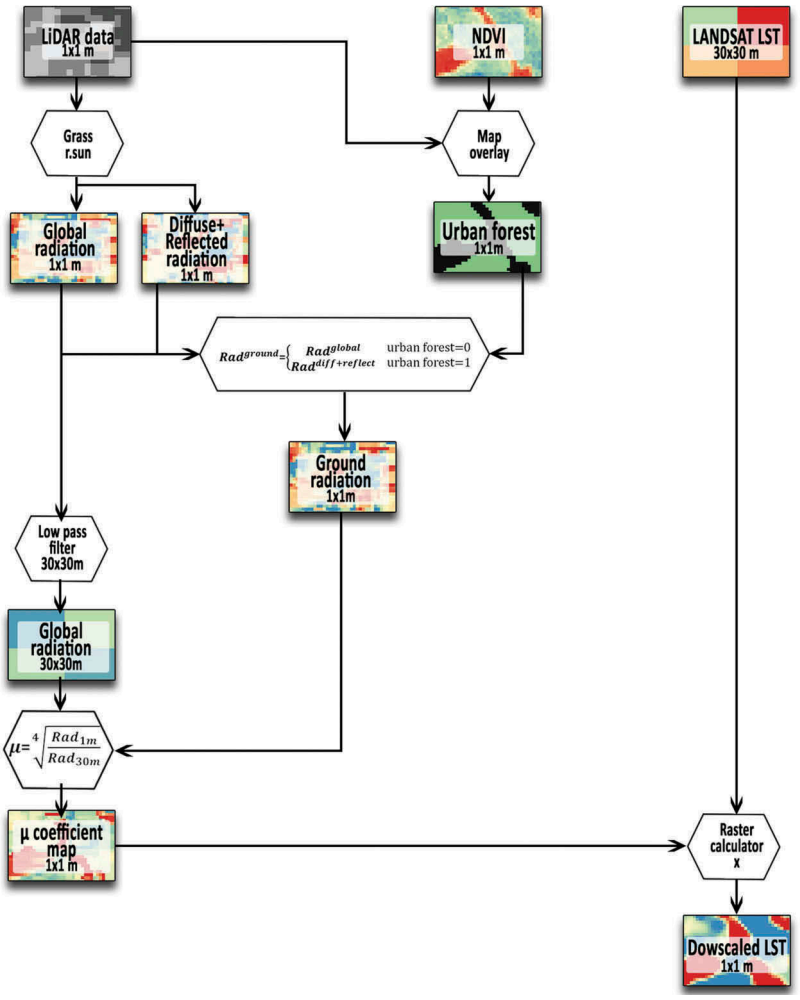

Figure 2. Graphical workflow.

$$\mu = \frac{(R^G)^{\frac{1}{4}}}{(R^T)^{\frac{1}{4}}},$$

where $\overline{R^T}$ is the mean of total radiation (direct + diffuse) calculated using a low pass filter with a kernel size of 30 m (equal to Landsat LST resolution):

$$\left(\overline{R^T}\right) = LowPass\underset{\text{size}=30m}{Filter}\left(R^T_{1m}\right).$$

At this stage of the workflow, it is necessary to apply the topographic indexes to the temperature maps. Because the LST map has a spatial resolution of 30 m, it was necessary to reduce the cell size to 25 m to make it compatible with the topographic index grids. We performed this procedure by means of spline interpolations, using the centers of each 30 m cell as data points. The last step is to multiply the two map sets (temperature and morphology indexes) to obtain the downscaled temperature maps.

LST with climate change

In this phase, we applied the original version of the method of Felicísimo Pérez and Martín-Tardío (2018) by downscaling the maps of maximum temperature of the warmest month (August) of the WorldClim dataset relative to the global climate model GFDL-ESM2G (670 × 930 m resolution) to the resolution of 30 m. Two maps were calculated for the RCP 2.6 and RCP 4.5 and scenarios of the IPCC V report. The downscaling of these maps to the resolution of the city LiDAR DEM (1 m) was performed by applying the procedure described in the previous paragraphs, assuming that climate change does not affect the survival of the urban forest.

Results and discussion

Figure 3 shows the aerial image of the study area (Figure 3(a)) and the two LST maps: the map calculated on the basis of the thermal band of the Landsat 8 satellite with a resolution of 30 m (Figure 3(b)) and the map calculated with the proposed procedure with 1 m resolution (Figure 3(c)).

Overall, excluding the obvious differences in geometric detail, the LST spatial models are similar: lower temperatures were recorded in the northern part of the study area, characterized by a greater density of urban tree vegetation, and higher temperatures were recorded in the southeast part of the area. The two maps differ, again in general terms,

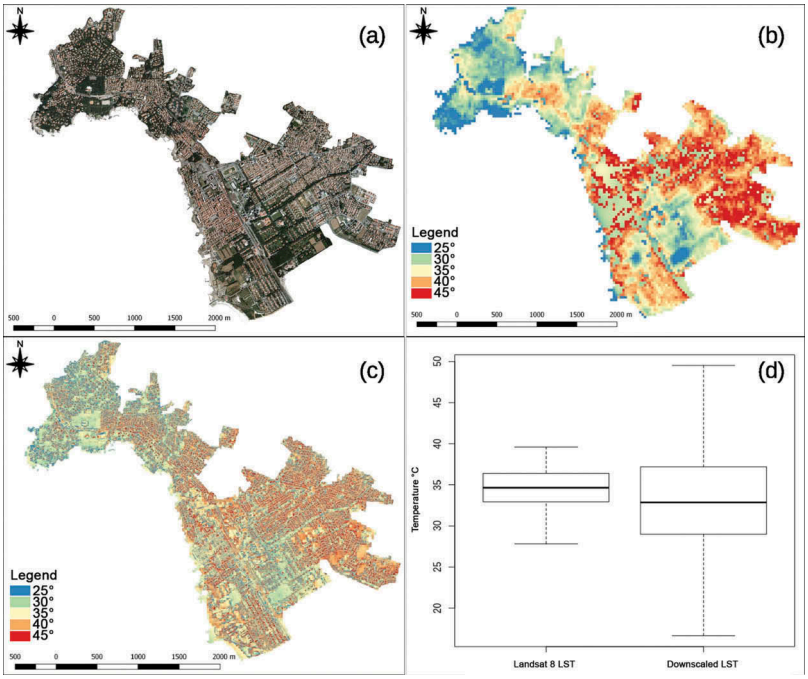

Figure 3. (a) visible image from aircraft; (b) LST from downscaling procedure with 1 m resolution; (c) LST from Landsat 8 data with 30 m pixels; (d) frequency distribution of downscaled LST and Landsat 8 LST.

in the frequency distribution of the LST, and the major difference emerges when observing the frequency distribution of temperature in the two maps (Figure 3(d)). Despite having similar average temperature (34.6°C for Landsat LST and 33.8°C for downscaled LST), the temperature distribution of the downscaled map has a greater range of variation than the temperatures derived by the Landsat 8 sensor. This is due primarily to the greater capacity of the downscaling method to detect differences due to the distribution of solar radiation according to the morphological characteristics of the city. In fact, the third quartile of the downscaled LST is slightly higher than that of the Landsat LST (37°C instead of 36°C). Moreover, the map derived by the downscaling procedure takes into account the shading caused by the tree vegetation at the level of the ground. For this reason, the first quartile of the distribution is lower than that of the Landsat LST (28°C instead of 32°C). In summary, our method is able to combine the satellite sensor's capability to detect temperature differences due to evapotranspiration with the power of 3D methods to consider the effect of city and urban green morphology.

The downscaled map also allows estimation of the effect of urban forest on the surface temperature in the public spaces of the city. Figure 4 shows box and whisker plots of the ground temperature distribution under the canopy of the trees compared to the temperature outside of the canopy in the squares and public streets of the study area.

The presence of the foliage of the trees provides a reduction in the median temperature value of about 7°C. Additionally, the range of temperature is reduced beneath the trees. In fact, under the canopy, the first and third quartiles of the temperature are 27°C and 31.3°C; however, outside of the shadow of the trees, these values are 32.8°C and 38.5°C, respectively.

The reduction of temperature in the public spaces becomes greater when considering the probable effects of climate change. Table 1 shows the temperature data with and without urban forest for the current climate, the RCP 2.6 scenario, and the RCP 4.5 scenario, respectively.

The median temperature in spaces in sunlight could rise to more than 38°C under the RCP 2.6 scenario and to almost 40°C under the RCP 4.5 scenario, with third quartile values of 41.1°C and 42.7°C, respectively. In the shadow of the urban forest, the median temperature should be maintained at 29.6°C (RCP 2.6) and 30.7°C (RCP 4.5), with third quartile values of 32°C (RCP 2.6) and 33.2°C (RCP 4.5).

The main utility of the downscaled LST is to have accurate information about the distribution of temperature on the hottest days at the city's design scale. For this reason, a detailed analysis was carried out on some urban patterns. To evaluate the impact of temperature on the well-being of people, the downscaled LST map was transformed into a bioclimatic well-being map through calculation of the discomfort index (*DI*) (Giles, Balafoutis, & Maheras, 1990; Honjo, 2009; Kyle, 1994):

$$DI = LST - (0.55 - 0.0055RH)(LST - 14.5),$$

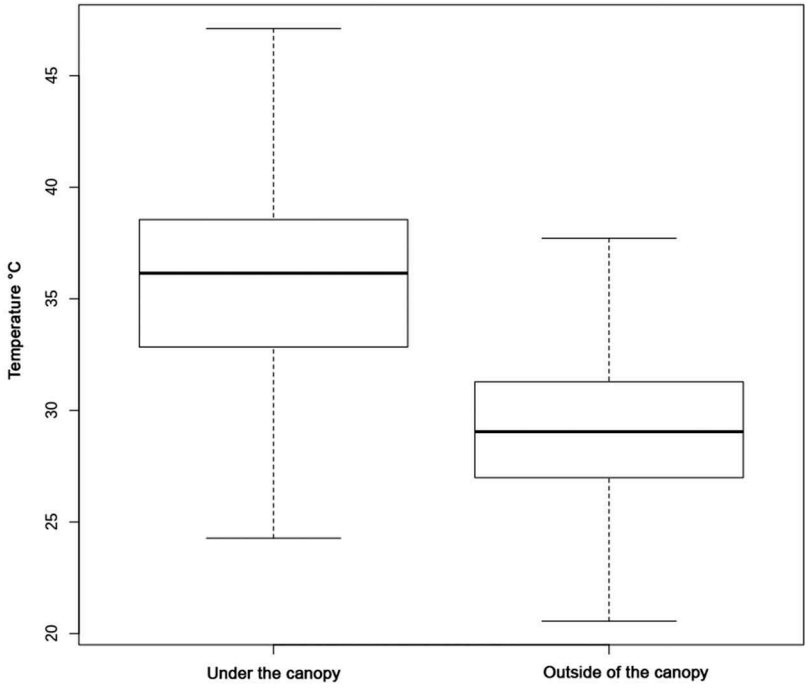

Figure 4. Box and whisker plots of the ground temperature distribution in the squares and public streets.

Table 1. Temperature data with and without urban forest for the current climate, RCP 2.6, and RCP 4.5.

Scenario	Urban forest	Mean	1st quartile	Median	3rd quartile
Curr. temp	Out of the canopy	35.5	32.8	36.1	38.5
Curr. temp	Under the canopy	29.3	27.0	29.0	31.3
RCP 2.6	Out of the canopy	37.3	34.4	38.3	41.1
RCP 2.6	Under the canopy	30.1	27.5	29.6	32.0
RCP 4.5	Out of the canopy	38.7	35.7	39.8	42.7
RCP 4.5	Under the canopy	31.3	28.5	30.7	33.2

where *RH* is percent relative humidity. For the relative humidity value of *RH* = 76.0%, data recorded by the weather station on 7 August 2007, the same date as the Landsat image used in the downscaling procedure, were used. Thom (1959) listed a series of boundary values indicating the degree of discomfort: DI less than 21, no discomfort (ND); DI from 21 to 24, less than 50% of the population feels discomfort (U50); DI from 24 to 27, more than 50% of the population feels discomfort (O50); DI from 27 to 29, most of the population suffers discomfort (MD); DI from 29 to 32, everyone feels severe stress (ES); and DI greater than 32, state of medical emergency (ME).

Figure 5 shows two avenues of the study area: the first with two rows of trees and the second without urban forest.

By examining the discomfort index maps, we can verify that most of the area of the road without trees falls into the classes of "severe stress" and "medical emergency." For the road with trees, the thermo-hygrometric comfort is instead mainly in the classes of "most of the population suffers discomfort" and "severe stress," with only the middle of the road in the "medical emergency" class.

The tree-lined road has a frequency distribution characterized by values that tend to be lower than

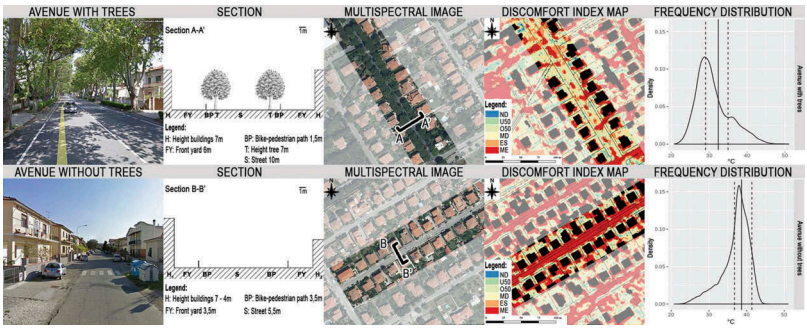

Figure 5. Urban pattern of an avenue with and an avenue without trees: ground view, section drawing, aerial view, discomfort index map and frequency distribution of temperature.

those of the road without vegetation. The median value of temperature (see also Table 2) is 30°C for the avenue with trees and 37.8°C for the avenue without vegetation. The third quartile temperature values are almost 40°C for the tree-less avenue but only 33.5°C for the tree-lined avenue. With regard to cooler locations, the first quartile temperature in the avenue with trees is 27.9°C, whereas this temperature is 35.5°C in the avenue without trees.

Figure 6 shows two squares with different tree species. In the first square, umbrella pine (*Pinus pinea* L.) and holm oak (*Quercus ilex* L.), with dense and shady foliage, were planted; in the second, oriental plane (*Platanus orientalis* L.), with light and sparse foliage, was used. The discomfort index map shows that the square with umbrella pine and holm oak has values ranging from "no discomfort" to "less than 50% of the population feels discomfort" for the areas under the foliage and values up to the classes of "severe stress" and "medical emergency" in the center of the square. In the square with oriental plane, the classes are the same, but there is less presence of areas within the classes "no discomfort" and "less than 50% of the population feels discomfort" and large surface area in the "medical emergency" class. In the square with the dense-canopy trees, the frequency distribution of temperature is bimodal, which clearly shows that there are cooler areas under the crowns of trees. In the square with light-canopy trees, the distribution is unimodal and left-skewed, and the presence of the trees is indicated only by the left tail of the frequency distribution. The position indexes (Table 2) indicate that the median temperature of the square with light-canopy trees is slightly higher (34.6°C) than that of the square with dense-canopy trees (32.4°C). However, there are greater differences for cooler areas. The first quantile temperature of the square with umbrella pine is 27.3°C, but the value of the square with oriental plane is 31.2°C.

The last case study (Figure 7) is represented by two urban woods: the city's castle park and the city's public park. The castle park is vegetated mainly by holm oak with some umbrella pine, whereas the trees in the public park are old umbrella pine. In both parks, the most represented classes of DI are "most of the population suffers discomfort" and "severe stress" and only a small area, outside of the shadow of the trees, falls into the "medical emergency" class. Additionally, the frequency distributions of temperature are similar: the median temperature values are 32°C for the castle park and 32.2°C for the public park. However, the frequency distribution of temperature of the castle park has a greater kurtosis due to the park's more homogeneous covering of foliage. The first and third quartiles of the castle park

Table 2. Position indexes of the distribution of LST temperature for the same urban patterns.

Scenario	Pattern	Mean	Median	1st quartile	3rd quartile
Current climate	Avenue with trees	31.1	30.0	27.9	33.5
Current climate	Avenue without trees	37.1	37.8	35.5	39.6
Current climate	Square with dense-canopy trees	31.3	32.5	27.3	34.8
Current climate	Square with light-canopy trees	33.2	34.6	31.2	35.9
Current climate	Public park	30.9	31.0	28.9	32.8
Current climate	Castle park	30.5	30.6	29.3	31.8
RCP 2.6	Avenue with trees	32.3	31.2	29.0	34.8
RCP 2.6	Avenue without trees	38.6	39.4	36.9	41.2
RCP 2.6	Square with dense-canopy trees	32.6	33.8	28.4	36.2
RCP 2.6	Square with light-canopy trees	34.6	36.0	32.4	37.3
RCP 2.6	Public park	32.3	32.2	29.7	34.4
RCP 2.6	Castle park	31.9	32.0	30.2	33.6
RCP 4.5	Avenue with trees	33.5	32.4	30.1	36.1
RCP 4.5	Avenue without trees	40.1	40.9	38.3	42.8
RCP 4.5	Square with dense-canopy trees	33.8	35.1	29.5	37.6
RCP 4.5	Square with light-canopy trees	35.9	37.4	33.7	38.7
RCP 4.5	Public park	33.6	33.4	30.8	35.8
RCP 4.5	Castle park	33.1	33.2	31.3	34.9

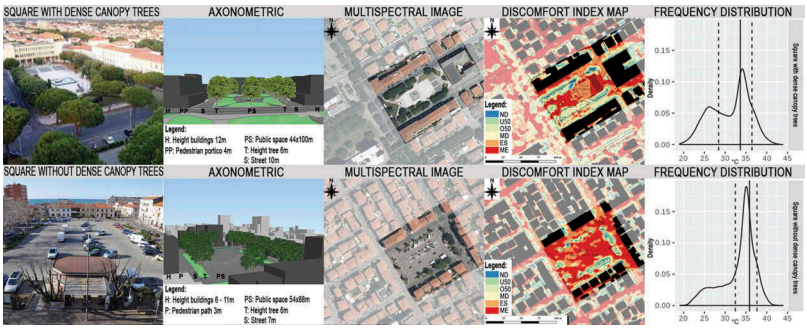

Figure 6. Two example squares with different species: ground view, perspective drawing, aerial view, discomfort index map and frequency distribution of temperature.

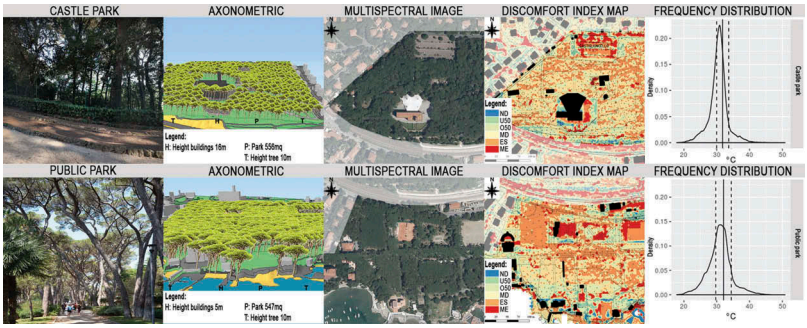

Figure 7. The castle park and the public park: ground view, perspective drawing, aerial view, discomfort index map and frequency distribution of temperature.

distribution are 30.2°C and 33.6°C whereas those for the public park are 29°C and 34.8°C, respectively.

Differences in the efficiency of patterns of urban forest in mitigating heat waves increase when climate change scenarios are considered. Table 2 shows that the presence of trees in the avenues could decrease the average temperature in 2050 by about 8°C: 32.3°C for the road with trees compared to 38.6°C for the road without trees under RCP 2.6°C and 33.5°C compared to 40.1°C under RCP 4.5. The different tree species used in the squares could result in a lower average temperature decrease of about 2°C: 34.6°C for the square with umbrella pine compared to 34.6°C for the square with oriental plane under RCP 2.6°C and 33.8°C compared to 35.9°C under RCP 4.5. However, the temperature difference is greater when considering the 1st quartile, corresponding to the areas under the canopy of the trees. The square with dense-foliage trees has a value of 28.4°C compared to a value of 32.4°C for the square with light-canopy trees under RCP 2.6°C and 29.5°C compared to 33.7°C under RCP 4.5. Finally, in the case of the two parks, it was found that this urban pattern has excellent capacity to mitigate the effects of climate change. In fact, the temperature increases of the two scenarios with respect to the current climate were decidedly low: just more than 1°C under RCP 2.6 and 2–3°C under RCP 4.5.

In conclusion, the analysis of the case studies demonstrated that urban forest has an important effect for mitigating the risks related to urban heat waves in both the current climate and under the future scenarios of climate change. In fact, for all of the sample areas, although conditions of real climatic well-being cannot exist under the foliage, it is possible to avoid situations of health risk. The results confirm those obtained in the literature with different methodologies. In general terms, the high-resolution maps achieved by with our downscaling method confirm the role of urban green in the mitigation of urban heat waves already investigated through medium resolution remote sensing methods (Aina et al. 2017; Maimaitiyiming et al., 2014; Weng & Schubring, 2004; Yuan & Bauer, 2007). Only a few studies have investigated the difference in surface temperature due to the shadow of urban trees and only through ground measured. Overall, the temperatures assessed by our methodology are similar in order of magnitude, to those recorded in the literature by ground measurements. Armson, Stringer, and Ennos (2012) examined the role that trees and grass can play in reducing temperatures (measured on the ground with an infrared thermometer) in urban areas during the summer within the urban landscape of Manchester, UK. The concrete surfaces reached peaks of about 40°C in the sun and 28°C in the shade, while the surface temperature of the grass was much lower, rising to peaks of around 23°C in the sun and 19°C to shadow. Tan et al. (2016) in high-density urban areas in Hong Kong measured (using a thermography camera) surface temperatures from 47.7°C to 52.8°C in road areas exposed to the sun and from 31.8°C to 34.4°C in road areas in the shade of trees. Finally, regarding the impact of climate change, Zölch, Maderspacher, Wamsler, and Pauleit (2016) investigated how different types and quantities of urban green infrastructure affect the thermal comfort of pedestrian high-density residential areas in current and future climatic conditions using the ENVI-met model with scenarios referring to the IPCC IV Report. The results obtained at the micro-scale are similar to those in the present study at city-scale and with IPCC V report: the trees shade the open spaces and provide evapotranspirant cooling with an average reduction in the physiological equivalent temperature of 13%.

Conclusions

The proposed method combines high-resolution remote sensing images with NIR band data, LiDAR data, Landsat 8 thermal sensor data, and weather station data to calculate high-resolution maps of LST in periods of heat wave. Using the data calculated by global climate models, we can also estimate the possible variations related to the climate change scenarios proposed by the IPCC V. The results demonstrated that the maps produced can provide useful information for the design of urban forests for the mitigation of urban heat wave. A limitation of the proposed methodology derives from

the image detected by the thermal sensor of the Landsat 8 referring to 10 a.m. which is probably not to the hottest hours of the day. This underestimation is however systematic and therefore does not affect the main objective of the work: to assess the temperature difference due to urban green on a heat wave day. However, it will be necessary to verify the possibility and errors of using morphological indices based on solar radiation calculated at different times of to project the Landsat LST to the hottest hours of the day. However, this work is only a first contribution to the study of the effects of urban forests on the city's microclimate and the climatic well-being of its population. The main limitations of the method and, consequently, future research needs follow. First, it is necessary to verify the reliability of the DI obtained through the downscaling method with the temperature effectively perceived by people. Therefore, in the next heat season, we expect to realize a survey through a questionnaire on thermal wellbeing (Lam, Loughnan, & Tapper, 2018; Lamarca, Qüense, & Henriquez, 2018). At the same time, field temperatures and relative humidity will be measured to verify the statistical error of the downscaling method. This survey will be performed on the basis of a stratified sampling in the study area based on the results of this work. Finally, an additional variable that will be analyzed is the effect of prevailing wind on the city's scale temperature.

Disclosure statement

No potential conflict of interest was reported by the authors.

ORCID

Iacopo Bernetti http://orcid.org/0000-0003-2297-1070

References

Acero, J.A., & Arrizabalaga, J. (2018). Evaluating the performance of ENVI-met model in diurnal cycles for different meteorological conditions. *Theoretical and Applied Climatology*, *131*(1–2), 455–469. doi:10.1007/s00704-016-1971-y

Aina, Y.A. (2017). Achieving smart sustainable cities with GeoICT support: The Saudi evolving smart cities. *Cities*, *71*, 49–58. doi:10.1016/j.cities.2017.07.007

Anderson, B.G., & Bell, M.L. (2009). Weather-related mortality: How heat, cold, and heat waves affect mortality in the United States. *Epidemiology (Cambridge, Mass.)*, *20*(2), 205. doi:10.1097/EDE.0b013e318190ee08

Armson, D., Stringer, P., & Ennos, A.R. (2012). The effect of tree shade and grass on surface and globe temperatures in an urban area. *Urban Forestry & Urban Greening*, *11*(3), 245–255. doi:10.1016/j.ufug.2012.05.002

Benestad, R.E., Hanssen-Bauer, I., & Chen, D. (2008). *Empirical-statistical downscaling*. World Scientific Publishing Company.

Bonafoni, S., Anniballe, R., Gioli, B., & Toscano, P. (2016). Downscaling landsat land surface temperature over the urban area of Florence. *European Journal of Remote Sensing*, *49*(1), 553–569. doi:10.5721/EuJRS20164929

Bowler, D.E., Buyung-Ali, L., Knight, T.M., & Pullin, A.S. (2010). Urban greening to cool towns and cities: A systematic review of the empirical evidence. *Landscape and Urban Planning*, *97*(3), 147–155. doi:10.1016/j.landurbplan.2010.05.006

Chun, B., & Guldmann, J.M. (2014). Spatial statistical analysis and simulation of the urban heat island in high-density central cities. *Landscape and Urban Planning*, *125*, 76–88. doi:10.1016/j.landurbplan.2014.01.016

D'Ippoliti, D., Michelozzi, P., Marino, C., De'Donato, F., Menne, B., Katsouyanni, K., … Atkinson, R. (2010). The impact of heat waves on mortality in 9 European cities: Results from the EuroHEAT project. *Environmental Health*, *9*(1), 37. doi:10.1186/1476-069X-9-37

Dunne, J.P., John, J.G., Adcroft, A.J., Griffies, S.M., Hallberg, R.W., Shevliakova, E., … Krasting, J.P. (2012). GFDL's ESM2 global coupled climate–Carbon earth system models. Part I: Physical formulation and baseline simulation characteristics. *Journal of Climate*, *25*(19), 6646–6665. doi:10.1175/JCLI-D-11-00560.1

Felicísimo Pérez, Á.M., & Martín-Tardío, M.Á. (2018). A method of downscaling temperature maps based on analytical hillshading for use in species distribution modelling. *Cartography and Geographic Information Science*, *45*(4), 329–338. doi:10.1080/15230406.2017.1338620

George, A.D., Thompson, F.R., III, & Faaborg, J. (2015). Using LiDAR and remote microclimate loggers to downscale near-surface air temperatures for site-level studies. *Remote Sensing Letters*, *6*(12), 924–932. doi:10.1080/2150704X.2015.1088671

Giles, B.D., Balafoutis, C., & Maheras, P. (1990). Too hot for comfort: The heatwaves in Greece in 1987 and 1988. *International Journal of Biometeorology*, *34*(2), 98–104.

Guo, G., Wu, Z., Xiao, R., Chen, Y., Liu, X., & Zhang, X. (2015). Impacts of urban biophysical composition on land surface temperature in urban heat island clusters. *Landscape and Urban Planning*, *135*, 1–10. doi:10.1016/j.landurbplan.2014.11.007

Hijmans, R.J., Cameron, S.E., Parra, J.L., Jones, P.G., & Jarvis, A. (2005). Very high resolution interpolated climate surfaces for global land areas. *International Journal of Climatology*, *25*(15), 1965–1978. doi:10.1002/(ISSN)1097-0088

Hodul, M., Knudby, A., & Ho, H. (2016). Estimation of continuous urban sky view factor from landsat data using shadow detection. *Remote Sensing*, *8*(7), 568. doi:10.3390/rs8070568

Honjo, T. (2009). Thermal comfort in outdoor environment. *Global Environmental Research*, *13*(2009), 43–47.

Isaya Ndossi, M., & Avdan, U. (2016). Application of open source coding technologies in the production of land surface temperature (LST) maps from Landsat: A PyQGIS plugin. *Remote Sensing*, *8*(5), 413. doi:10.3390/rs8050413

Kokalj, Ž., Zakšek, K., & Oštir, K. (2011). Application of sky-view factor for the visualisation of historic landscape features in lidar-derived relief models. *Antiquity*, *85*(327), 263–273. doi:10.1017/S0003598X00067594

Konijnendijk, C.C. (2003). A decade of urban forestry in Europe. *Forest Policy and Economics*, *5*(2), 173–186. doi:10.1016/S1389-9341(03)00023-6

Kyle, W.J. (1994, August). The human bioclimate of Hong Kong. In proceedings of the contemporary climatology conference, Brno. TISK LITERA, Brno (pp. 345–350). *Meteorology*, *16*(1), 11–19.

Lam, C.K.C., Loughnan, M., & Tapper, N. (2018). Visitors' perception of thermal comfort during extreme heat events at the Royal Botanic Garden Melbourne. *International Journal of Biometeorology*, *62*(1), 97–112. doi:10.1007/s00484-015-1125-4

Lamarca, C., Qüense, J., & Henriquez, C. (2018). Thermal comfort and urban canyons morphology in coastal temperate climate, Concepción, Chile. *Urban Climate*, *23*, 159–172. doi:10.1016/j.uclim.2016.10.004

Lenzholzer, S., & Brown, R.D. (2016). Post-positivist microclimatic urban design research: A review. *Landscape and Urban Planning*, *153*, 111–121. doi:10.1016/j.landurbplan.2016.05.008

Maimaitiyiming, M., Sagan, V., Tiyip, T., Pla, F., Carmona, P., Halik, Ü., … Caetano, M. (2014). Effects of green space spatial pattern on land surface temperature: Implications for sustainable urban planning and climate change adaptation. *ISPRS Journal of Photogrammetry and Remote Sensing*, *89*, 59–66. doi:10.1016/j.isprsjprs.2013.12.010

Mirzaei, P.A. (2015). Recent challenges in modeling of urban heat island. *Sustainable Cities and Society*, *19*, 200–206. doi:10.1016/j.scs.2015.04.001

Mitasova, H., & Neteler, M. (2008). *Open source GIS: A GRASS GIS approach*. Switzerland, AG: Springer.

Myrup, L.O. (1969). A numerical model of the urban heat island. *Journal of Applied Meteorology*, *8*(6), 908–918. doi:10.1175/1520-0450(1969)008<0908:ANMOTU>2.0.CO;2

Nakata-Osaki, C.M., Souza, L.C.L., & Rodrigues, D.S. (2018). THIS–Tool for Heat Island Simulation: A GIS extension model to calculate urban heat island intensity based on urban geometry. *Computers, Environment and Urban Systems*, *67*, 157–168. doi:10.1016/j.compenvurbsys.2017.09.007

Nunez, M., & Oke, T.R. (1977). The energy balance of an urban canyon. *Journal of Applied Meteorology*, *16*(1), 11–19.

Oke, T.R. (1973). City size and the urban heat island. *Atmospheric Environment (1967)*, *7*(8), 769–779. doi:10.1016/0004-6981(73)90140-6

Oke, T.R. (1988). The urban energy balance. *Progress in Physical Geography*, *12*(4), 471–508. doi:10.1177/030913338801200401

Rajeshwari, A., & Mani, N.D. (2014). Estimation of land surface temperature of dindigul district using Landsat 8 data. *International Journal of Research in Engineering and Technology*, *3*(5), 122–126. doi:10.15623/ijret.2014.0305025

Rizwan, A.M., Dennis, L.Y., & Chunho, L.I.U. (2008). A review on the generation, determination and mitigation of urban heat island. *Journal of Environmental Sciences*, *20*(1), 120–128. doi:10.1016/S1001-0742(08)60019-4

Roth, M., Oke, T.R., & Emery, W.J. (1989). Satellite-derived urban heat islands from three coastal cities and the utilization of such data in urban climatology. *International Journal of Remote Sensing*, *10*(11), 1699–1720. doi:10.1080/01431168908904002

Rozbicki, T., & Golaszewski, D. (2003, September). Analysis of local climate changes in Ursynów in the period 1960–1991 as a result of housing estate development. In Proc. 5th Int. Conf. urban climate (Vol.2, pp. 455–458).

Salvati, A., Monti, P., Roura, H.C., & Cecere, C. (2019). Climatic performance of urban textures: Analysis tools for a Mediterranean urban context. *Energy and Buildings*, *185*, 162–179. doi:10.1016/j.enbuild.2018.12.024

Scarano, M., & Sobrino, J.A. (2015). On the relationship between the sky view factor and the land surface temperature derived by Landsat-8 images in Bari, Italy. *International Journal of Remote Sensing*, *36*(19–20), 4820–4835. doi:10.1080/01431161.2015.1070325

Tan, Z., Lau, K.K.L., & Ng, E. (2016). Urban tree design approaches for mitigating daytime urban heat island effects in a high-density urban environment. *Energy and Buildings*, *114*, 265–274. doi:10.1016/j.enbuild.2015.06.031

Thom, E.C. (1959). The discomfort index. *Weatherwise*, *12*(2), 57–61. doi:10.1080/00431672.1959.9926960

Trzaska, S., & Schnarr, E. (2014). A review of downscaling methods for climate change projections: African and Latin American resilience to climate change (ARCC).

Weng, Q., Lu, D., & Schubring, J. (2004). Estimation of land surface temperature–Vegetation abundance relationship for urban heat island studies. *Remote Sensing of Environment*, *89*(4), 467–483. doi:10.1016/j.rse.2003.11.005

Yuan, F., & Bauer, M.E. (2007). Comparison of impervious surface area and normalized difference vegetation index as indicators of surface urban heat island effects in Landsat imagery. *Remote Sensing of Environment*, *106*(3), 375–386. doi:10.1016/j.rse.2006.09.003

Zhao, C., Jensen, J., Weng, Q., & Weaver, R. (2018). A geographically weighted regression analysis of the underlying factors related to the surface urban heat island phenomenon. *Remote Sensing*, *10*(9), 1428. doi:10.3390/rs10091428

Zölch, T., Maderspacher, J., Wamsler, C., & Pauleit, S. (2016). Using green infrastructure for urban climate-proofing: An evaluation of heat mitigation measures at the micro-scale. *Urban Forestry & Urban Greening*, *20*, 305–316. doi:10.1016/j.ufug.2016.09.011